(revision 1, October 2012, "The American Mineralogist" manuscript 4143)

Calibration of zircon as a Raman spectroscopic pressure sensor to high temperatures and application to water-silicate melt systems

C. Schmidt[1,*], M. Steele-MacInnis[2], A. Watenphul[3], and M. Wilke[1]

[1]Deutsches GeoForschungsZentrum (GFZ), Section 3.3 Chemistry and Physics of Earth Materials, Telegrafenberg, D-14473 Potsdam, Germany

[2]Department of Geosciences, Virginia Tech, Blacksburg, VA 24061, USA

[3]Hamburger Synchrotronstrahlungslabor HASYLAB at Deutsches Elektronen-Synchrotron DESY, Notkestr. 85, 22607 Hamburg, Germany

*E-mail: hokie@gfz-potsdam.de

Abstract - The shifts in wavenumber of the $\nu_3(SiO_4)$ (~1008 cm^{-1}) Raman band of fully crystalline synthetic zircon with changing pressure (P) and temperature (T) were calibrated for application as a Raman spectroscopic pressure sensor in optical cells to about 1000 °C and 10 GPa. The relationship between wavenumber (ν) of this band and T from 22 to 950 °C is described by the equation $\nu[cm^{-1}] = 7.54 \cdot 10^{-9} \cdot T^3 - 1.61 \cdot 10^{-5} \cdot T^2 - 2.89 \cdot 10^{-2} \cdot T + 1008.9$, where T is given in [°C]. The pressure dependence is nearly linear over the studied range in P. At ~25 °C, the $\partial\nu/\partial P$ slope to 6.6 GPa is 5.69 cm^{-1}/GPa, and that to 2 GPa is 5.77 cm^{-1}/GPa. The $\partial\nu/\partial P$ slope does not significantly change with temperature, as determined from experiments conducted along isotherms up to 700 °C. Therefore, this pressure sensor has the advantage that a constant $\partial\nu/\partial P$ slope of 5.8±0.1 cm^{-1}/GPa can be applied in experiments to pressures of at least about 6.6 GPa without introducing a significant error. The pressure sensor was tested to determine isochores in experiments with H_2O+$Na_2Si_3O_7$ and H_2O+$NaAlSi_3O_8$ fluids to 803 °C and 1.65 GPa. These pressures were compared to pressures calculated from the EoS of

H_2O based on the measured vapor dissolution or ice melting temperature for the same experiment. Pressures determined from the zircon sensor in runs in which $NaAlSi_3O_8$ melt dissolved in aqueous fluid were close to or lower than the pressure calculated from the EoS of H_2O using the vapor dissolution or ice melting temperature. In experiments with H_2O+Na_2O+SiO_2 fluids, however, the pressure obtained from the Raman spectrum of zircon was often significantly higher than that estimated from the EoS of H_2O. This suggests that the pressures along some critical curves of water–silicate melt pseudobinary systems should be revised.

Keywords: zircon, Raman spectroscopy, temperature, pressure sensor, diamond anvil cell

1. Introduction

Experiments using diamond-anvil cells have been pivotal in many studies of minerals and fluids at high pressure (P) and temperature (T) because these cells permit not only optical observation of the sample but also *in situ* measurement of physical and chemical properties by "photon-in – photon-out" techniques. The pressure in the sample chamber of such cells must be determined indirectly, which is commonly done by measurement of the liquid-vapor homogenization temperature of the fluid pressure medium with application of an appropriate equation of state or using the shift in wavenumber of a Raman or fluorescence line of a calibrant inside the sample chamber. However, fluorescence intensities decrease rapidly with increasing temperature, such that Raman lines are the often better option for pressure determination at elevated temperatures, particularly above 400 °C. The $^5D_0$–$^7F_0$ fluorescence line of SrB_4O_7:Sm^{2+} is still detectable at 627 °C, but this pressure sensor is quite soluble in aqueous fluids (Datchi et al. 2007). The 464 cm^{-1} Raman line of quartz is often applied to determine pressure because of its large shift with P ($\partial\nu/\partial P$ ~9 cm^{-1}/GPa) and relatively small shift with T ($\partial\nu/\partial T$ ~-0.014 cm^{-1}/deg) (Schmidt and Ziemann 2000). However, its use is

limited by phase transitions and high solubility of quartz in many fluids and melts. The wavenumber difference between two Raman lines of berlinite, $AlPO_4$, is more sensitive to pressure than that of the 464 cm^{-1} Raman line of quartz, and its determination does not require a high-resolution Raman spectrometer, but berlinite reacts readily with aqueous fluids (Watenphul and Schmidt 2012). In situations in which quartz or berlinite are not suitable for use as spectroscopic pressure sensors, zircon is one alternative because it is stable over a large range in *P*, *T*, and fluid composition (e.g., Watson and Harrison 1983). Other inert Raman spectroscopic calibrants such as ^{13}C diamond or cubic boron nitride (*c*-BN) display only small wavenumber shifts with pressure of ~2.83 cm^{-1}/GPa (first-order Raman line, Schiferl et al. 1997; Datchi et al. 2007), or ~3.27 cm^{-1}/GPa (TO mode, Datchi and Canny 2004), and also fairly large and nonlinear shifts in the wavenumber with temperature. This makes the application of ^{13}C diamond or *c*-BN more difficult at relatively low pressures because of limitations in the attainable accuracy and precision in determining wavenumbers and actual sample temperatures. As described in the following sections, zircon offers the advantage over these phases that the shift in the wavenumber of its most intense Raman line with pressure is about twice as large as those of *c*-BN and ^{13}C-diamond.

The four most intense Raman bands of zircon (Fig. 1) at wavenumbers >300 cm^{-1} have been assigned to internal vibrations of the SiO_4 tetrahedra. Specific assignments include $\nu_3(SiO_4)$ (antisymmetric stretching mode) to the band at 1008 cm^{-1}, $\nu_1(SiO_4)$ (symmetric stretching mode) to the band at 975 cm^{-1}, $\nu_2(SiO_4)$ (symmetric bending mode) to the band at 439 cm^{-1}, and $\nu_4(SiO_4)$ (antisymmetric bending mode) or an external lattice mode to the band at 356 cm^{-1} (Dawson et al. 1971; Syme et al. 1977; Nasdala et al. 2003). Although there is a large number of Raman spectroscopic studies on zircon, very few data are available on its Raman band parameters as functions of pressure and temperature. The effect of pressure on the positions of these bands and on the linewidth of $\nu_3(SiO_4)$ has previously been characterized at ambient temperature for fully crystalline and radiation-damaged zircon (Knittle and Williams

1993, Nasdala et al. 2008), and that of temperature on positions and linewidths at -183 °C and 22 °C by Syme et al. (1977). To our knowledge, such data are lacking for elevated temperatures. In addition, there is significant disagreement on the $\partial\nu/\partial P$ slope of the $\nu_3(SiO_4)$ band, i.e., 5.9 cm^{-1}/GPa (Nasdala et al. 2008, synthetic zircon) vs. 4.8±0.2 cm^{-1}/GPa (Knittle and Williams 1993, natural zircon with little radiation damage).

In this study, we calibrated zircon as Raman spectroscopic pressure sensor for experiments using diamond-anvil or other optical cells, particularly for experiments at high temperatures and with fluid compositions in which the spectrosopic pressure sensors quartz and berlinite are readily dissolved and can no longer be applied. For this application, we focused on the shift in the wavenumber of the $\nu_3(SiO_4)$ band with pressure and temperature, because it has the largest $\partial\nu/\partial P$ slope of Raman bands of zircon (Knittle and Williams 1993). In addition, this band is very intense in most crystallographic orientations of the zircon relative to the direction of polarization of the laser (its intensity is only zero at $\boldsymbol{E} \parallel$ c and the incident beam $\perp$ {110}, Dawson et al. 1971). Additional objectives were to test if fully crystalline zircon persists in H_2O+Na_2O+SiO_2±Al_2O_3 fluids at high P and T, and to compare pressures calculated from EoS of H_2O to pressures determined from Raman spectra of zircon in experiments with H_2O + silicate melts.

2. Methods

The zircon sample was synthesized in an 1 atm furnace from 500 mg of oxide mixture (10.8 mass% ZrO_2, 26.8 mass% SiO_2, and 62.4 mass% PbO as flux) and seeds of natural crystalline Hf-bearing zircon in a Pt crucible using a temperature ramp from 1430 to 1350 °C at 1 deg/h with subsequent quench, followed by treatment with 48% hydrofluoric acid to remove excess quartz. Electron microprobe analyses gave the following mean composition (mass%) SiO_2 32.73 ± 0.36, HfO_2 1.48 ± 0.31, ZrO_2 66.40 ± 0.28 (46 analyses). This corresponds to a composition of $Zr_{0.987}Hf_{0.013}[SiO_4]$. Lead was present in low concentrations in some analyses,

but was mostly below the detection limit. The backscattered electron images of the sample verified its compositional homogeneity.

All spectra recorded for calibration of the zircon Raman spectrum were acquired using a HORIBA Jobin Yvon LabRAM HR800 UV-Vis Raman spectrometer (gratings 1800 lines/mm, focal length 800 mm, confocal pinhole aperture set at 100 μm to reduce the background from the diamond anvils, excitation by 488 nm line of an Ar^+ laser), equipped with a CCD-detector (1024 × 256 pixel) and an Olympus microscope. The unpolarized spectra were obtained in backscattering geometry using 20× objectives with long working distances of 25 mm or 20.5 mm to avoid damage to the objectives from heat transfer during experiments at high temperature. For each spectrum, the positions of the studied Raman bands of zircon and of the pressure calibrant quartz (464 cm^{-1} quartz Raman line) were calibrated based on the plasma lines from the Ar^+ laser at 1057.25 cm^{-1} (514.5319 nm) and 737.49 cm^{-1} (506.2036 nm), or 380.40 cm^{-1} (497.2157 nm), 351.70 cm-1 (496.5073 nm), and 221.60 cm^{-1} (493.3206 nm). This was achieved by removal of the interference filter to record the plasma lines and the Raman bands in the same spectrum, without a change in the spectrometer settings. The use of the 488 nm line for excitation had the advantage that the plasma lines at 1057.25 cm^{-1} (514.5319 nm) and 737.49 cm^{-1} (506.2036 nm) and the $\nu_1(SiO_4)$ and $\nu_3(SiO_4)$ Raman bands of zircon could be recorded in the same spectral window. The spectral resolution was about 0.9±0.1 cm^{-1} based on the line width of the recorded plasma lines. All spectra from the calibration runs were processed using the software package PeakFit v4.11 from SYSTAT Software Inc. The Raman lines of quartz were fitted with the asymmetric model Pearson IV. The Raman lines of zircon and the plasma lines from the laser were fitted with the symmetric Gauss+Lorentz area function using a linear baseline correction in the selected section. The range in the wavenumber of the sections used to fit the $\nu_1(SiO_4)$ and $\nu_3(SiO_4)$ Raman bands of zircon is given in Tab. 1. This resulted in good fits with insignificant or small nonstatistical residuals. The accuracy in the determined peak positions

is about ±0.1 to ±0.2 cm^{-1}. No temperature reduction for the Bose-Einstein occupation factor was performed before fitting the spectrum profile. Note that application of other functions to fit the Raman bands of zircon gives normally very similar results for the wavenumber, but this is not always the case for the line width. In addition, deviations in wavenumber due to different applied functions for band fitting have no significant effect on determined pressure if the shift in the wavenumber relative to that at a reference *P* and *T* is measured.

Raman spectra of zircon as a function of temperature at atmospheric pressure were recorded using a Linkam TS1000 heating stage. The temperature was calibrated based on optical observation of melting of a small halite crystal (800.7 °C at 0.1 MPa) near the center of a Pt crucible, which itself was close to the center of heated ceramic crucible of the stage. Subsequently, a small zircon chip was then placed at the same location at which halite melting had been observed. This was done to minimize potential effects of temperature gradients. Raman spectra were then obtained at various temperatures beween 22 to 950 °C with a NIKON M Plan SLWD 20× objective (numerical aperture 0.35). The output laser power set via the laser controller was 200 mW, which corresponded to a measured laser power of 34.0 mW "downstream" of the objective. These measurements were verified by additional measurements at temperatures between 25 and 741 °C using an externally-heated Bassett-type hydrothermal diamond-anvil cell (HDAC) (Bassett et al. 1993), the design of which had been modified to improve the accuracy of temperature measurements. This cell was equipped with type Ia ultra-low fluorescence and ultra-low birefringence grade diamond anvils (culet diameter 0.9 mm). The temperature in the sample chamber of the cell was measured using K-type (Ni/NiCr) thermocouples attached to the diamond anvils. These thermocouples were calibrated using the α-β transition temperature of quartz (574 °C, 0.1 MPa) and the triple point of H_2O (0.01 °C, 0.6 kPa). The power input to the resistive heaters was controlled using Eurotherm® 2408 temperature controllers, which held the set temperature within ± 0.2 °C. Accuracy and reproducibility of the temperature measurements were about ± 0.1 to ± 0.2 °C

157 at ~20 °C and usually better than ± 1 °C at temperatures between 100 and 600 °C (Schmidt
158 2009). Other conditions for recording the Raman spectra of zircon and the plasma lines were
159 the same as those during the run using the Linkam TS1000 heating stage, except that the
160 output laser power set via the laser controller was 300 mW.
161 The same HDAC was used to obtain Raman spectra of zircon as a function of pressure up to
162 1.95 GPa at ambient temperature. Zircon and quartz crystals were loaded into the sample
163 chamber (a hole with an initial diameter of ~400 μm in a Re gasket that separated the
164 diamond anvils) together with distilled water as pressure medium. The pressure was increased
165 incrementally by stepwise compression of the sample chamber. The pressure was determined
166 by recording Raman spectra of quartz immediately before and after that of zircon and using
167 the average of the pressures obtained from the wavenumber shift of the 464 cm^{-1} Raman line
168 of quartz based on Eq. (2) of Schmidt and Ziemann (2000). A NIKON M Plan SLWD 20×
169 objective (numerical aperture 0.35) was used, and the output laser power set via the laser
170 controller was 300 mW, which corresponded to approximately 30 mW in the sample
171 chamber. Another series of experiments at about 23 °C and pressures up to 6.6 GPa was
172 carried out using a megabar-type piston-cylinder diamond-anvil cell (DAC) (Mao and
173 Hemley 1998) with type IIa low fluorescence diamond anvils with culet size of 400 μm.
174 Chips of zircon and quartz and annealed ruby spheres were loaded into the sample chamber,
175 which consisted of a hole of 200 μm diameter in a pre-indented stainless steel gasket. A
176 16:3:1 mixture of methanol, ethanol, and distilled water was used as pressure medium to
177 ensure hydrostatic conditions. Similarly to the HDAC experiments as function of pressure at
178 ambient temperature, the pressure was incrementally increased by stepwise compression of
179 the sample chamber, and spectra of zircon, quartz, and ruby were collected for each pressure
180 step. An OLYMPUS SLMPlan N 20× objective (numerical aperture 0.25) was used. The
181 output laser power set via the laser controller was 206 mW, which corresponded to a
182 measured laser power of 40.4 mW "downstream" of the objective. For recording the strong R_1

fluorescence line of ruby, the laser power was decreased by a factor of 1000 by inserting a filter. This also ensured that no laser heating of the ruby spheres occurred. Watenphul and Schmidt (2012) showed that pressures determined from the calibrated wavenumber shift of the 464 cm^{-1} Raman line of quartz using equation (2) of Schmidt and Ziemann (2000) remain in good agreement to pressures of at least 10 GPa with pressures obtained from the shift of the R_1 ruby fluorescence line using pressure dependencies determined by Piermarini et al. (1975). Therefore, the pressure for this run series are from the shift of the 464 cm^{-1} Raman line of quartz, with verification by the pressures from the shift of the R_1 fluorescence line of ruby (using the calibration by Piermarini et al. 1975). The deviations of these pressures from those determined from quartz remained small, but increased from approximately -0.01 GPa at the lowest pressure to approximately +0.25 GPa at the highest pressure of this series.

For the experiments at simultaneously elevated pressures and temperatures, we used the same HDAC as for the run at 0.1 MPa to 741 °C and for the series at 27 °C to 1.95 GPa, except that the upper anvil was replaced by a synthetic type IIa ultra-low fluorescence grade diamond anvil (culet diameter 0.9 mm). The measured temperature was calibrated as described for the run at 0.1 MPa to 741 °C. Chips of the zircon sample and natural quartz, and distilled water were loaded into the HDAC sample chamber, for which an iridium gasket was used to ensure that the gasket material remained inert during the experiment at high temperature and pressure. The sample chamber was sealed and heated to 600 °C to clean the chamber and the loaded crystals by reaction of possible fluorescence-causing organic contaminants with water to form methane (Schmidt 2009). After cooling, the sample chamber was opened, and fresh distilled water was loaded. Before it was sealed again, an air bubble was allowed to grow by controlled leaking until the desired approximate initial fluid density was attained. The sample was then studied by visual observation and Raman spectroscopy at different temperatures and pressures along a near isochoric pressure–temperature path. Then, the fluid density was changed by adjusting of the liquid-vapor ratio, and data along the next near isochoric path

were collected. Data at three to four different pressures were obtained for each isotherm (300, 400, 500, 600, and 700 °C) and for one experiment at 200 °C. The pressure at elevated temperature was determined from the measured liquid-vapor homogenization temperature after isochoric cooling and the IAPWS 1995 equation of state of H_2O (Wagner and Pruß 2002). At temperatures up to 500 °C, the wavenumber shift of the 464 cm^{-1} Raman line of quartz (Schmidt and Ziemann 2000; equations (2) and (3) therein) was used for additional pressure determination. At these conditions, the concentration of dissolved silica is relatively small, and the pressure from both methods was in good agreement as expected, and as already noted by Schmidt and Watenphul (2010) for an experiment with quartz and water to 600 °C, 920 MPa. The resolution (random uncertainty) of the pressure determination from the wavenumber shift of the 464 cm^{-1} Raman line of quartz was about 25 MPa (Schmidt 2009). During the runs, the cell was flushed with 99% Ar + 1% H_2 gas to prevent oxidation of metallic parts. The objective was an OLYMPUS SLMPlan N 20× (numerical aperture 0.25), and the output laser power set via the laser controller 206 mW (40.4 mW measured in the focal point of the objective). Additional data at 200 °C, 360 MPa and 300 °C, 304 MPa were obtained from a run using spectroscopic grade ethanol as pressure medium, for which the pressure was determined from the wavenumber shift of the 464 cm^{-1} Raman line of quartz (Schmidt and Ziemann, 2000) and emission lines from a Ne lamp were used to calibrate the wavenumber.

In all run series, reference Raman spectra of the solids in the sample chambers of the heating stage or pressure cell (diamond-anvil cell) were acquired at ~0.1 MPa and ambient temperature at the start of the series. In the runs using a diamond-anvil cell, trapping of a small air bubble when the sample chamber was sealed ensured the low reference pressure. Additional reference spectra were acquired in these experiments at the end of the series, after pressure release.

The zircon pressure sensor was tested during HDAC experiments on H_2O+$NaAlSi_3O_8$ and H_2O+$Na_2Si_3O_7$ fluids. Details of those studies will be reported elsewhere, whereas here we will only discuss the outcomes of using the zircon pressure sensor. Note that the same zircon sample was used in all of these experiments, and the bulk composition was determined using the method described by Manning et al. (2008). Specifically, the mass of the doubly polished silicate glass piece loaded into the sample chamber was calculated from its determined volume and its known density. The mass of the added water was calculated from the volume of the sample chamber, less the volumes of glass and zircon chips, and its density as obtained from the liquid-vapor homogenization temperature upon first heating. All volumes were obtained by optical micrometry. The Raman spectra of the test experiments were recorded using HORIBA Jobin Yvon LabRAM HR800 Raman spectrometers (gratings 1800 lines/mm, focal length 800 mm, excitation by the 514.53 nm line of an Ar^+ laser or by the 472.937 nm line from a diode laser), and the wavenumber was calibrated using emission lines from a Ne lamp.

3. Results

Table 1 lists the data for the wavenumbers and the linewidth (FWHM = full width at half maximum) of the $\nu_3(SiO_4)$ Raman band of zircon as function of temperature and pressure. The temperature dependence of the position of the $\nu_3(SiO_4)$ Raman band at 0.1 MPa is shown in Figure 2. Two different heating stages were used, a Linkam TS1000 and a HDAC. There is good agreement between both series, although temperature gradients in the sample chambers were certainly different. Because of the larger range in temperature, the data obtained using the Linkam TS1000 were used to fit the relationship between wavenumber v of the $\nu_3(SiO_4)$ Raman band of fully crystalline zircon and temperature T at 0.1 MPa

$$v[\mathrm{cm}^{-1}] = 7.54(88)*10^{-9}*T^3 - 1.61(13)*10^{-5}*T^2 - 2.89(5)*10^{-2}*T + 1008.90(6) \quad (1)$$

where $22 < T\ [°C] < 950$. Numbers in parentheses denote 1σ errors in last significant digits. The deviation of wavenumbers calculated from Eqn (1) and data from the run using the Linkam TS1000 stage is between -0.12 cm^{-1} and 0.11 cm^{-1}, mostly $\leq \pm 0.05$ cm^{-1}. The deviation of wavenumbers calculated from Eqn (1) and data from the other experiments at 0.1 MPa using the HDAC or DAC ranges from -0.45 cm^{-1} to 0.34 cm^{-1}.

Within the uncertainty of the data, the $v_3(SiO_4)$ (~1008 cm^{-1} at ambient temperature) Raman band of synthetic zircon displayed a linear change in wavenumber with changing pressure (Fig. 3). At 23 °C, the obtained $\partial v/\partial P$ slope of the $v_3(SiO_4)$ band is 5.69 cm^{-1}/GPa based on the data from the DAC experiments to the maximum pressure of 6.6 GPa. Slight nonlinearity may be inferred from the increase in that slope to 5.76 cm^{-1}/GPa if only the data to 2.52 GPa are included in the linear fit. This is confirmed by the slope of 5.77 cm^{-1}/GPa from the HDAC series to 1.98 GPa at 27 °C (Fig. 3). Figure 4 shows that the $\partial v/\partial P$ slope does not significantly change with T, as determined for the 700 and 600 °C isotherms ($\partial v/\partial P$ ~5.81 and 5.89 cm^{-1}/GPa). The $\partial v/\partial P$ slopes along other isotherms (300, 400, and 500 °C) do not differ by much from these values, but are less reliable because of the smaller range in pressure and are therefore given in parentheses in Fig. 4.

In this study, we focused on the shift in the wavenumber of the of the $v_3(SiO_4)$ (~1008 cm^{-1}) Raman band. Therefore, results for the linewidth of the $v_3(SiO_4)$ band and results for other Raman bands are only briefly summarized here. In the following, these Raman bands v_i will be denoted by their approximate position at ambient conditions, i.e., v_{975}, v_{439}, v_{356}, v_{224}, v_{214}, and v_{202}. Their positions and widths as function of temperature and pressure are listed in the electronic appendix (Table 2). Additionally, Fig. 5 shows a series of Raman spectra recorded at various temperatures and constant pressure (0.1 MPa). At 0.1 MPa, the v_{439} band displays the largest increase in the full width at half maximum with temperature from ~5 cm^{-1} at 22 °C to ~24 cm^{-1} at 900 °C. The increases in the linewidths of the Si–O stretching bands v_{1008} and v_{975} with temperature at 0.1 MPa are moderate, from ~2 cm^{-1} at 22 °C to ~13 cm^{-1} at 900 °C.

285 The FWHM of the ν_{356} band increases from ~4 cm^{-1} at 22 °C to ~18 cm^{-1} at 900 °C, that of the
286 ν_{224} band from ~3 cm^{-1} at 22 °C to ~12 cm^{-1} at 900 °C, that of the ν_{214} band from ~3 cm^{-1} at 22
287 °C to ~14 cm^{-1} at 900 °C, and the FWHM of the ν_{202} band shows the smallest increase from
288 ~1 cm^{-1} at 22 °C to ~4 cm^{-1} at 900 °C. The temperature dependencies of the wavenumbers of
289 of the Si–O stretching bands ν_{1008} and ν_{975} at 0.1 MPa are distinctly nonlinear, whereas those
290 of the ν_{439}, ν_{356}, ν_{224}, ν_{214}, and ν_{202} bands are close to linear. In the following, the $\partial v/\partial T$ slopes
291 at 22 and 700 °C are reported in the case of nonlinear behavior to enable comparison between
292 different Raman bands. The ν_{1008} band shows the largest wavenumber decrease with
293 temperature at 0.1 MPa. The first derivative of Eqn (1) gives -0.0296 cm^{-1}/deg at 22 °C and -
294 0.0404 cm^{-1}/deg at 700 °C. The $\partial v/\partial T$ slopes at 0.1 MPa of the other bands are -0.0194 cm^{-1}/deg at 22 °C and -0.0240 cm^{-1}/deg at 700 °C for the ν_{975}, -0.0166 cm^{-1}/deg for ν_{439} , -0.0187
296 cm^{-1}/deg for ν_{356} (-0.0147 cm^{-1}/deg at 22 °C and -0.0196 cm^{-1}/deg at 700 °C), -0.0056 cm^{-1}/deg for ν_{224}, -0.0105 cm^{-1}/deg for ν_{214} (-0.0092 cm^{-1}/deg at 22 °C and -0.0112 cm^{-1}/deg at
298 700 °C), and -0.0034 cm^{-1}/deg for the ν_{202} band (-0.0022 cm^{-1}/deg at 22 °C and -0.0042 cm^{-1}/deg at 700 °C). The isothermal change in the wavenumber with pressure is nearly constant
300 for all studied Raman bands. At 23 °C, the obtained $\partial v/\partial P$ slopes for the data to 6.6 GPa are
301 5.69 cm^{-1}/GPa for the $\nu_{1008} = \nu_3(SiO_4)$ band (Fig. 3), 5.16 cm^{-1}/GPa for ν_{975}, 1.45 cm^{-1}/GPa for
302 ν_{439}, 4.56 cm^{-1}/GPa for ν_{356}, 0.22 cm^{-1}/GPa for ν_{224}, 1.45 cm^{-1}/GPa for ν_{214}, and -0.45 cm^{-1}/GPa for the ν_{202} band. As determined for the ν_{1008} band, the $\partial v/\partial P$ slopes of the ν_{975}, ν_{356},
304 ν_{224}, ν_{214}, and ν_{202} bands at 23°C do likewise not differ significantly from the $\partial v/\partial P$ slopes
305 along other isotherms (500, 600, and 700 °C). The $\partial v/\partial P$ slope of the ν_{439} band may be
306 dependent on temperature because the slopes along the 300, 400, 500, 600, and 700 °C
307 isotherms are slightly but consistently smaller than that at 23 °C. Observed changes in the
308 linewidths of the ν_{975}, ν_{439}, ν_{356}, ν_{224}, ν_{214}, and ν_{202} Raman bands with pressure along isotherms
309 are probably mostly insignificant (Tab. 1 and electronic appendix (Tab. 2)).

The zircon pressure sensor was applied to determine isochores for aqueous fluids with 6, 35, or 37 mass% $NaAlSi_3O_8$ (Figs. 6a-c), and 11, 26, or 61 mass% $Na_2Si_3O_7$ (Figs. 6d-f) to 803 °C and 1.65 GPa. This was done along cooling *P-T* paths, for which the sample chamber volume usually remains constant (Bassett et al. 1993; Schmidt and Ziemann 2000). In the case of the $NaAlSi_3O_8$ dissolution experiments in water, the difference between the isochores from the zircon sensor and the isochores calculated from the liquid-vapor homogenization temperature using the EoS of H_2O (Wagner and Pruß 2002) was small or insignificant to about 700 °C. Above this temperature, the pressure from the zircon pressure sensor increased less with temperature than the pressure from the EoS of H_2O in the experiments with the bulk compositions H_2O + 35 mass% $NaAlSi_3O_8$ and H_2O + 37 mass% $NaAlSi_3O_8$ (Figs. 6b-c). For experiments with H_2O + $Na_2Si_3O_7$, the d*P*/d*T* slopes of the isochores obtained from zircon were about the same or steeper than those calculated from homogenization temperature and EoS of H_2O (Figs. 6d-f). The largest observed difference between both pressures was ~520 MPa at 500 °C in the experiment with H_2O + 61 mass% $Na_2Si_3O_7$ (Fig. 6f). None of the calibration and few of the test experiments with H_2O+SiO_2±Na_2O±Al_2O_3 fluids pointed to a high zircon solubility. Fairly high zircon solubilities were indicated in an experiment with H_2O + 80 mass% $Na_2Si_3O_7$, in which ~0.26 vol% zircon dissolved completely upon heating to 600 °C at ~500 MPa, a run with a H_2O+6 mol% Na_2O+7 mol% SiO_2 fluid, in which ~0.3 vol% zircon dissolved completely at 600 °C and ~900 MPa, and a run with a H_2O+6 mol% Na_2O+4 mol% SiO_2 fluid, in which ~0.89 vol% zircon dissolved completely at 600 °C and ~1400 MPa. Furthermore, there was no optical and Raman spectroscopic detection of formation of secondary Zr-oxides or Zr-silicates in any of these runs.

4. Discussion and Conclusions

There is close agreement in the obtained $\partial\nu/\partial P$ slopes of the $\nu_3(SiO_4)$ band for different isotherms (5.76 cm^{-1}/GPa at 23 °C to 2.52 GPa, 5.77 cm^{-1}/GPa at 27 °C to 1.98 GPa, 5.89 cm^{-}

336 ^{1}/GPa at 600 °C to 1.05 GPa, and 5.81 cm^{-1}/GPa at 700 °C to 1.24 GPa), although the
337 pressures were determined using different techniques. The results indicate that the shift in the
338 position of the $\nu_3(SiO_4)$ band with changing pressure is close to constant ($\partial\nu/\partial P$ = 5.8±0.1 cm^{-}
339 ^{1}/GPa) and independent of temperature over the whole range in pressures and temperatures
340 studied here. The possible slightly nonlinear behavior was not taken into account because it is
341 within the error of the linear approximation of ±0.1 cm^{-1}/GPa, which corresponds to ±0.12
342 GPa at 7 GPa.
343 This nearly linear, fairly large, and temperature-independent shift of the $\nu_3(SiO_4)$ band with
344 pressure is only one argument for the suitability of crystalline zircon as pressure sensor for
345 experiments using optical cells at high *P* and *T*. Zircon is of particular advantage in situations
346 where other phases cannot be used as pressure sensors because of phase transitions or high
347 solubility. Diamond-anvil cell experiments at ambient temperature showed that synthetic
348 zircon transforms into reidite at 19.7 GPa (Van Westrenen et al. 2004). This pressure should
349 be higher than the equilibrium transition pressure (Knittle and Williams 1993). The transition
350 pressure determined by Liu (1979) is 12 GPa at 1027 °C. Ono et al. (2004) found a positive
351 $\partial P/\partial T$ slope of the phase boundary between zircon and reidite (8.33 GPa at 827 °C, 8.67 GPa
352 at 1027 °C). This indicates that zircon should be applicable as Raman spectroscopic pressure
353 sensor to pressures of ~10 GPa even at elevated temperature or, in other words, over most of
354 the range in *P* and *T* relevant for experiments on aqueous fluids at subduction zone
355 conditions.
356 However, the wavenumber of the $\nu_3(SiO_4)$ Raman band also depends on the degree of
357 radiation-induced disorder and the crystallite size of recrystallized zircon (e.g., Nasdala et al.
358 1995, Zhang et al. 2000; Geisler and Pidgeon 2002) and on the composition, e.g., it increases
359 substantially with the Hf concentration (~0.12 cm^{-1}/mol% $HfSiO_4$, Hoskin and Rodgers 1996;
360 0.13 cm^{-1}/mol% $HfSiO_4$, own data) and decreases with addition of Th (e.g., Syme et al.,
361 1977). The Zr–Hf ratio in the zircon used in this study was very close to the estimated atomic

ratio of the crustal abundances of Zr and Hf of about 70:1, and natural zircons do usually not deviate much from this ratio (Finch and Hanchar 2003, and references therein). Therefore, most natural zircons with little radiation-damage can also be used as Raman spectroscopic pressure sensor. Systematic errors in pressure determination, e.g., induced by the composition of natural zircon samples, can be eliminated by measuring the shift in the wavenumber of the $\nu_3(SiO_4)$ Raman band as wavenumber difference $\Delta\nu$ relative to the position of that band at ambient temperature and low (near atmospheric) pressure in the same sample. It needs to be emphasized that the actual sample temperature should be well known for accurate determination of P using this sensor because of the temperature sensitivity of the wavenumber ($\partial\nu/\partial T$ is ~-0.03 cm^{-1}/deg at 22 °C and ~-0.04 cm^{-1}/deg at $T \geq 500$ °C). This temperature sensitivity may be the largest source of error in the application of zircon as Raman spectroscopic pressure sensor. The largest deviations of wavenumbers from experiments at 0.1 MPa using the HDAC (Tab. 1) and wavenumbers calculated from Eqn (1), which is based on the data from experiments using the Linkam TS1000 heating stage, were 0.16 cm^{-1} and -0.45 cm^{-1}, respectively. These deviations in wavenumber correspond to deviations in pressure of +28 and -78 MPa, but include small systematic errors related to temperature measurement and calibration. Deviations in the wavenumber of data at ambient temperature range between -0.08 to 0.34 cm^{-1}. We therefore consider ± 50 MPa to be a reasonable estimate of the reproducibility and random error of this technique.

An additional advantage of using zircon as a pressure sensor is its chemical durability at most conditions. As an amphoteric element, zirconium is more soluble in acidic or basic fluids than at near neutral pH. However, the solubility of crystalline zircon in H_2O+HCl is rather moderate, ~10^{-2} m_{Zr} at 500 °C in ~7 m HCl (Schmidt et al. 2006). In aqueous fluids, zircon is stable below quartz saturation, but not at very low silica activities (e.g., Newton et al. 2005). The solubility of zircon in hydrous peraluminous andesitic to granitic melts is low, ~100 to 1330 ppm Zr at 750 to 1020 °C and 120 to 600 MPa (Watson and Harrison 1983). At 700–

800 °C, 200 MPa, the solubility of zircon is below 100 ppm Zr in felsic peraluminous hydrous melts in the system SiO_2-Al_2O_3-Na_2O-K_2O, but increases strongly and linearly as function of increasing alkali/aluminum ratio, with up to 3.9 mass% Zr dissolved at $(Na_2O+K_2O)/Al_2O_3$=2.0 (Watson 1979). In our study, the highest congruent zircon solubility was observed in a test experiment, in which 0.89 vol% zircon dissolved completely at 600 °C and ~1400 MPa in a highly alkaline aqueous fluid (H_2O+6 mol% Na_2O+4 mol% SiO_2).

An obvious application of zircon as Raman spectroscopic pressure sensor are studies of hydrous silicate melts or other systems for which α-quartz is of limited applicability due to phase transitions and high solubility. It has long been suspected that pressures in such experiments may not be well approximated by the EoS of H_2O due to the considerable excess volume of mixing in such systems (e.g., Mysen and Wheeler 2000). However, until recently pressures estimated from the EoS of H_2O had to be assumed in studies of hydrous silicate melts, because an appropriate spectroscopic pressure sensor for use in such experiments was lacking (e.g., Shen and Keppler 1997; Bureau and Keppler 1999; Manning et al. 2008; Borchert et al. 2009, 2010). The isochores determined in this study in experiments on mixtures of aqueous fluids and silicate melts using the zircon sensor demonstrate that high mutual solubility of fluid and melt can have a significant effect on the *P-V-T* properties. Application of the EoS of H_2O (Wagner and Pruß 2002) appears to yield good or reasonable approximations of the actual pressure for low concentrations of dissolved $NaAlSi_3O_8$. If more than about 10 mass% $NaAlSi_3O_8$ was dissolved in the aqueous fluid, the isochores deviated towards lower pressure from those calculated from the EoS of H_2O (Figs. 6b-c). The situation is different for H_2O + $Na_2Si_3O_7$ mixtures, for which the pressure from the EoS of H_2O was often much lower than the actual pressure, particularly at high concentrations of dissolved sodium silicate (Fig. 6f) and at relatively high bulk densities (Figs. 6d and 6f). The results of these tests suggest that it may be worthwile to revise phase equilibria involving aqueous fluid

413 and silicate melt, e.g., to redetermine the *P*-*T* location of critical curves in pseudobinary
414 systems such as those studied by Shen and Keppler (1997) and Bureau and Keppler (1999).
415
416 **Acknowledgments**
417 The authors thank Christopher Beyer for the synthesis and Oona Appelt and Dieter Rhede for
418 the electron microprobe analyses of the zircon sample, Maria Mrosko and Monika Koch-
419 Müller for providing the DAC, Alan Anderson and Ross Angel for discussions, and Boriana
420 Mihailova, I-Ming Chou, and an anonymous reviewer for their suggestions to improve an
421 earlier version of the manuscript. Financial support for Matthew Steele-MacInnis was
422 provided by the Institute for Critical Technology and Applied Science (ICTAS) at Virginia
423 Tech.
424
425 **REFERENCES CITED**
426 Bassett, W.A., Shen, A.H., Bucknum, M., and Chou, I-M. (1993) A new diamond anvil cell
427 for hydrothermal studies to 2.5 GPa and from -190 to 1200 °C. Reviews of Scientific
428 Instruments, 64, 2340–2345.
429 Borchert, M., Wilke, M. Schmidt, C., and Rickers-Appel, K. (2009) Partitioning and
430 equilibration of Rb and Sr between silicate melts and aqueous fluids. Chemical Geology, 259,
431 39–47.
432 Borchert, M., Wilke, M., Schmidt, C., Cauzid, J., and Tucoulou, R. (2010) Partitioning of Ba,
433 La, Yb and Y between haplogranitic melts and aqueous solutions: An experimental study.
434 Chemical Geology, 276, 225–240.
435 Bureau, H. and Keppler, H. (1999) Complete miscibility between silicate melts and hydrous
436 fluids in the upper mantle; experimental evidence and geochemical implications. Earth and
437 Planetary Science Letters, 165, 187–196.

438 Datchi, F. and Canny, B. (2004) Raman spectrum of cubic boron nitride at high pressure and
439 temperature. Physical Review B, 69, 144106, 1–7.
440 Datchi, F., Dewaele, A., Loubeyre, P., LeToullec, R., Le Godec, Y., and Canny, B. (2007)
441 Optical pressure sensors for high-pressure–high-temperature studies in a diamond anvil cell.
442 High Pressure Research, 27, 447–463.
443 Dawson, P., Hargreave, M.M., and Wilkinson, G.R. (1971) The vibrational spectrum of
444 zircon ($ZrSiO_4$). Journal of Physics C: Solid State Physics, 4, 240-256.
445 Finch, R.J. and Hanchar, J.M. (2003) Structure and chemistry of zircon and zircon-group
446 minerals. Reviews in Mineralogy and Geochemistry, 53, 1-25.
447 Geisler, T. and Pidgeon, R.T. (2002) Raman scattering from metamict zircon: Comments on
448 "Metamictisation of natural zircon: accumulation versus thermal annealing of radioactivity-
449 induced damage" by Nasdala et al., 2001 (Contributions to Mineralogy and Petrology, 141,
450 125-144). Contributions to Mineralogy and Petrology 143, 750-755.
451 Hoskin, P.W.O. and Rodgers, K.A. (1996) Raman spectral shift in the isomorphous series
452 $(Zr_{1-x}Hf_x)SiO_4$. European Journal of Solid State and Inorganic Chemistry 33, 1111-1121.
453 Knittle, E. and Williams, Q. (1993) High-pressure Raman spectroscopy of $ZrSiO_4$:
454 Observation of the zircon to scheelite transition at 300 K. American Mineralogist, 78, 245-
455 252.
456 Liu, L. (1979) High-pressure phase transformations in baddeleyite and zircon, with
457 geophysical implications. Earth and Planetary Science Letters, 72, 433-439.
458 Manning, C.E., Wilke, M., Schmidt, C., and Cauzid, J. (2008) Rutile solubility in albite-H_2O
459 and $Na_2Si_3O_7$-H_2O at high temperatures and pressures by in-situ synchrotron radiation micro-
460 XRF. Earth and Planetary Science Letters, 272, 730-737.
461 Mao, H.-K. and Hemley, R.J. (1998) New windows on the Earth's deep interior. Reviews in
462 Mineralogy and Geochemistry, 37, 1-32.

463 Mysen, B.O. and Wheeler, K. (2000) Alkali aluminosilicate-saturated fluids in the earth's
464 upper mantle. Geochimica et Cosmochimica Acta, 64, 4243–4256.
465 Nasdala, L., Wolf, D., and Irmer, G. (1995) The degree of metamictization in zircon: a Raman
466 spectroscopic study. European Journal of Mineralogy, 7, 471-478.
467 Nasdala, L., Zhang, M., Kempe, U., Panczer, G., Gaft, M., Andrut, M., and Plötze, M. (2003)
468 Spectroscopic methods applied to zircon. Reviews in Mineralogy and Geochemistry, 53, 427-
469 467.
470 Nasdala, L., Miletich, R., Ruschel, K., and Váczi, T. (2008) Raman study of radiation-
471 damaged zircon under hydrostatic compression. Physics and Chemistry of Minerals, 35, 597–
472 602.
473 Newton, R.C., Manning, C.E., Hanchar, J.M., and Finch, R.J. (2005) Gibbs Free Energy of
474 formation of zircon from measurement of solubility in H_2O. Journal of the American Ceramic
475 Society, 88, 1854-1858.
476 Ono, S., Funakoshi, K., Nakajima, Y., Tange, Y., and Katsura, T. (2004) Phase transition of
477 zircon at high P-T conditions. Contributions to Mineralogy and Petrology, 147, 505-509.
478 Piermarini, G.J., Block, S., Barnett, J.D., and Forman, R.A. (1975) Calibration of the pressure
479 dependence of the R_1 ruby fluorescence line to 195 kbar. Journal of Applied Physics, 46,
480 2774-2780.
481 Schiferl, D., Nicol, M., Zaug, J.M., Sharma, S.K., Cooney, T.F., Wang, S.-Y., Anthony, T.R.,
482 and Fleischer, J.F. (1997) The diamond $^{13}C/^{12}C$ isotope Raman pressure sensor system for
483 high temperature/pressure diamond-anvil cells with reactive samples. Journal of Applied
484 Physics, 82, 3256–3265.
485 Schmidt, C. (2009) Raman spectroscopic study of a $H_2O + Na_2SO_4$ solution at 21–600 °C and
486 0.1 MPa to 1.1 GPa: Relative differential ν_1-SO_4^{2-} Raman scattering cross sections and
487 evidence of the liquid–liquid transition. Geochimica et Cosmochimica Acta 73, 425-437.

Schmidt, C. and Ziemann, M.A. (2000) In-situ Raman spectroscopy of quartz: A pressure sensor for hydrothermal diamond-anvil cell experiments at elevated temperatures. American Mineralogist, 85, 1725-1734.

Schmidt, C., Rickers, K., Wirth, R., Nasdala, L., and Hanchar, J.M. (2006) Low-temperature Zr mobility: An in situ synchrotron-radiation XRF study of the effect of radiation damage in zircon on the element release in H_2O + HCl ± SiO_2 fluids. American Mineralogist, 91, 1211-1215.

Schmidt, C. and Watenphul, A. (2010) Ammonium in aqueous fluids to 600 °C, 1.3 GPa: A spectroscopic study on the effects on fluid properties, silica solubility, and K-feldspar to muscovite reactions. Geochimica et Cosmochimica Acta, 74, 6852–6866.

Shen, A. and Keppler, H. (1997) Direct observation of complete miscibility in the albite-H_2O system. Nature, 385, 710–712.

Syme, R.W.G., Lockwood, D.J., and Kerr, H.J. (1977) Raman spectrum of synthetic zircon ($ZrSiO_4$) and thorite ($ThSiO_4$). Journal of Physics C: Solid State Physics, 10, 1335-1348.

Van Westrenen, W., Frank, M.R., Hanchar J.M., Fei, Y., Finch R.J., and Zha, C.-S. (2004) In situ determination of the compressibility of synthetic pure zircon ($ZrSiO_4$) and the onset of the zircon-reidite phase transition. American Mineralogist, 89, 197-203.

Wagner, W. and Pruß, A. (2002) The IAPWS formulation 1995 for the thermodynamic properties of ordinary water substance for general and scientific use. Journal of Physical and Chemical Reference Data, 31, 387–535.

Watenphul, A. and Schmidt, C. (2012) Calibration of berlinite ($AlPO_4$) as Raman spectroscopic pressure sensor for diamond-anvil cell experiments at elevated temperatures. Journal of Raman Spectroscopy, 43, 564–570.

Watson, E.B. (1979) Zircon saturation in felsic liquids: experimental results and applications to trace element geochemistry. Contributions to Mineralogy and Petrology, 70, 407-419.

513 Watson, E.B. and Harrison, T.M. (1983) Zircon saturation revisited: temperature and
514 composition effects in a variety of crustal magma types. Earth and Planetary Science Letters,
515 64, 295-304.
516 Zhang, M., Salje, E.K.H., Farnan, I., Graeme-Barber, A., Daniel P., Ewing, R.C., Clark,
517 A.M., and Lennox, H. (2000) Metamictization of zircon: Raman spectroscopic study. Journal
518 of Physics: Condensed Matter, 12, 1915-1925.

519

520 **Figure captions**

521

522 Fig. 1. Raman spectrum of synthetic fully crystalline zircon (near endmember composition
523 $Zr_{0.987}Hf_{0.013}[SiO_4]$) at 22 °C, 0.1 MPa, with band assignments. Arrows indicate the direction
524 of the shift in the wavenumber of these bands with temperature and pressure.

525

526 Fig. 2. Position of the $\nu_3(SiO_4)$ Raman band of zircon vs. temperature at 0.1 MPa. Errors are
527 smaller than the symbol size. The solid line represents the fit of the data measured using the
528 Linkam TS1000. The given equation is valid for $22 \leq T\ [°C] \leq 950$.

529

530 Fig. 3. Position of the $\nu_3(SiO_4)$ Raman band of zircon vs. pressure at ~22 °C (DAC
531 experiment) and ~27 °C (HDAC experiment). Errors are smaller than the symbol size. Solid
532 lines represent linear fits of the data. Numbers refer to the slopes of these linear equations.
533 Details are given in the text.

534

535 Fig. 4. Position of the $\nu_3(SiO_4)$ Raman band of zircon vs. pressure along isotherms from 27 to
536 700 °C (HDAC experiments, pressure determined from EoS of H_2O (Wagner and Pruß 2002)
537 and/or quartz as Raman spectroscopic pressure sensor (Schmidt and Ziemann 2000)). Values
538 for the $\partial\nu/\partial P$ slopes are obtained from linear fits (solid and dashed lines). If these values are

more uncertain because of the more limited pressure range, the lines are dashed and the numbers for the $\partial\nu/\partial P$ slopes are given in parentheses.

Fig. 5. Series of Raman spectra of synthetic fully crystalline zircon ($Zr_{0.987}Hf_{0.013}[SiO_4]$) recorded at various temperatures and 0.1MPa using the Linkam TS1000. The spectra are shifted along the intensity axis, but are not normalized to the acquisition time or to the temperature based on the Bose-Einstein occupation factor. * = plasma lines from laser.

Fig. 6. Isochores determined from the zircon pressure sensor (thick grey lines and symbols, diamonds = individual pressure determinations) using the calibration from this study, and isochores (thick black lines) and densities from the EoS of H_2O (Wagner and Pruß 2002). Dashed lines – isochores for the same bulk composition, but at a lower density. Also shown are *P-T* conditions of phase transitions (vapor dissolution or ice I melting, and silicate melt dissolution (circles), qz = quartz. The estimated uncertainty in pressure from the $\nu_3(SiO_4)$ Raman band of zircon is ± 50 MPa (about symbol size). (**a**) H_2O + 6 mass % $NaAlSi_3O_8$, (**b**) H_2O + 35 mass % $NaAlSi_3O_8$, (**c**) H_2O + 37 mass % $NaAlSi_3O_8$, (**d**) H_2O + 11 mass % $Na_2Si_3O_7$, (**e**) H_2O + 26 mass % $Na_2Si_3O_7$, (**f**) H_2O + 61 mass % $Na_2Si_3O_7$.

Table 1. Experimentally determined wavenumber and linewidth of the $\nu_3(SiO_4)$ Raman band of fully crystalline synthetic zircon ($Zr_{0.987}Hf_{0.013}[SiO_4]$) as functions of temperature and pressure.

T [°C]	*P* [MPa]	$\nu_3(SiO_4)$ [cm^{-1}]	$\Gamma\nu_3(SiO_4)$ [cm^{-1}]	section [cm^{-1}]	$T_{LV=L}$ [°C]	experimental details
22	0.1	1008.15	2.3	950–1050		TS1000
50	0.1	1007.43	2.5	950–1050		TS1000
100	0.1	1005.92	2.7	950–1050		TS1000
150	0.1	1004.34	3.1	950–1050		TS1000
200	0.1	1002.56	3.6	925–1075		TS1000
250	0.1	1000.83	4.0	925–1075		TS1000
300	0.1	998.96	4.5	875–1100		TS1000
350	0.1	997.16	5.0	875–1100		TS1000
400	0.1	995.17	5.6	875–1100		TS1000

450	0.1	993.29	6.2	875–1100	TS1000
500	0.1	991.30	6.8	875–1100	TS1000
550	0.1	989.34	7.5	875–1100	TS1000
600	0.1	987.37	8.2	875–1100	TS1000
650	0.1	985.36	8.8	875–1100	TS1000
700	0.1	983.43	9.5	875–1100	TS1000
750	0.1	981.47	10.5	850–1100	TS1000
800	0.1	979.31	11.1	825–1125	TS1000
850	0.1	977.37	12.0	825–1125	TS1000
900	0.1	975.25	12.9	825–1125	TS1000
950	0.1	973.34	13.9	825–1125	TS1000
25.5	0.1	1008.23	2.7	950–1050	HDAC
25.3	0.1	1008.04	2.7	950–1050	HDAC
98.8	0.1	1006.13	3.1	950–1050	HDAC
98.8	0.1	1005.91	3.3	950–1050	HDAC
197.6	0.1	1002.56	4.0	925–1075	HDAC
197.6	0.1	1002.92	3.7	925–1075	HDAC
296.4	0.1	999.32	4.6	875–1100	HDAC
395.2	0.1	995.87	5.6	875–1100	HDAC
494	0.1	991.59	6.8	875–1100	HDAC
592.9	0.1	987.95	8.1	875–1100	HDAC
691.6	0.1	984.16	9.5	875–1100	HDAC
741	0.1	982.11	10.2	850–1100	HDAC
26.8	0.1	1007.95	2.6	950–1050	HDAC,W
26.5	46	1008.35	2.5	950–1050	HDAC,W,Q
26.5	88	1008.47	2.6	950–1050	HDAC,W,Q
26.2	173	1009.08	2.6	950–1056	HDAC,W,Q
26.3	265	1009.67	2.7	950–1056	HDAC,W,Q
26.6	440	1010.61	2.6	950–1056	HDAC,W,Q
26.5	606	1011.55	2.6	955–1056	HDAC,W,Q
26.6	874	1013.00	2.6	955–1056	HDAC,W,Q
26.6	1100	1014.46	2.9	960–1056	HDAC,W,Q
26.7	1264	1015.32	2.6	960–1056	HDAC,W,Q
26.7	1439	1016.48	2.8	960–1056	HDAC,W,Q
27.0	1303	1015.75	2.6	960–1056	HDAC,W,Q
26.9	1682	1017.87	2.7	960–1056	HDAC,W,Q
26.8	1682	1017.83	2.7	960–1056	HDAC,W,Q
27.0	1948	1019.23	2.8	960–1056	HDAC,W,Q
26.9	1948	1019.31	2.8	960–1056	HDAC,W,Q
26.7	1978	1019.35	2.7	950–1075	HDAC,W,Q
24.2	0.1	1007.85	2.3	950–1075	DAC,MEW
23.1	41	1008.04	2.3	950–1075	DAC,MEW,Q
22.8	241	1009.33	2.4	950–1075	DAC,MEW,Q
22.9	1217	1014.76	2.3	950–1075	DAC,MEW,Q
23.0	1503	1016.49	2.3	950–1075	DAC,MEW,Q
23.1	2516	1022.39	2.2	950–1075	DAC,MEW,Q
23.2	3258	1026.43	2.2	950–1080	DAC,MEW,Q
23.2	3953	1030.34	2.2	950–1085	DAC,MEW,Q
23.2	4403	1032.87	2.3	950–1085	DAC,MEW,Q
23.2	4903	1035.89	2.2	950–1085	DAC,MEW,Q

23.2	5579	1039.83	2.2	950–1090		DAC,MEW,Q
23.3	6126	1042.87	2.2	950–1090		DAC,MEW,Q
23.4	6645	1045.29	2.4	950–1090		DAC,MEW,Q
23.4	44	1008.09	2.2	950–1075		DAC,MEW,Q
21.8	0.1	1008.19	2.2	950–1050		HDAC,W
200	120	1003.39	3.5	900–1075	131.7	HDAC,W,EoS
200	360	1004.42	3.6	950–1040		HDAC,E,Q
300	9	999.22	4.5	875–1100	P_V	HDAC,W,EoS
300	149	1000.00	4.5	875–1100	206.8	HDAC,W,EoS
300	310	1000.83	4.4	875–1100	131.7	HDAC,W,EoS
300	304	1000.71	4.5	940–1050		HDAC,E,Q
400	108	995.88	5.5	875–1100	303.9	HDAC,W,EoS
400	309	997.22	5.5	875–1100	206.8	HDAC,W,EoS
400	502	998.17	5.5	875–1100	131.7	HDAC,W,EoS
500	213	992.67	6.7	875–1100	303.9	HDAC,W,EoS
500	466	994.17	6.7	875–1100	206.8	HDAC,W,EoS
500	854	996.42	6.6	875–1100	71.4	HDAC,W,EoS
500	652	995.40	6.6	875–1100	144.0	HDAC,W,EoS
600	316	989.30	8.1	875–1100	303.9	HDAC,W,EoS
600	618	991.01	8.0	875–1100	206.8	HDAC,W,EoS
600	1052	993.53	8.0	875–1100	71.4	HDAC,W,EoS
600	829	992.37	8.0	875–1100	144.0	HDAC,W,EoS
700	437	985.79	9.5	875–1100	298.1	HDAC,W,EoS
700	765	987.88	9.6	875–1100	206.8	HDAC,W,EoS
700	1242	990.59	9.4	900–1100	71.4	HDAC,W,EoS

Notes: T = temperature; P = pressure; $v_3(SiO_4)$ = determined wavenumber of the $v_3(SiO_4)$ Raman band of zircon; $\Gamma v_3(SiO_4)$ = full width at half maximum of the $v_3(SiO_4)$ Raman band of zircon (not corrected for spectral resolution); section [cm^{-1}] = section of the spectrum used to fit the $v_1(SiO_4)$ and $v_3(SiO_4)$ Raman bands (plasma lines were omitted and fitted individually); $T_{LV=L}$ = liquid-vapor homogenization temperature of the aqueous pressure medium after isochoric cooling. P_V = experiment at vapor pressure. TS1000 = Linkam TS1000 heating stage, HDAC, = hydrothermal diamond-anvil cell, DAC = piston-cylinder diamond-anvil cell. Pressure medium: W = water; MEW = 16:3:1 mixture of methanol, ethanol, and distilled water; E = ethanol. Pressure determination technique: Q = wavenumber shift of the 464 cm^{-1} Raman line of quartz using equation (2) of Schmidt and Ziemann (2000); EoS = liquid-vapor homogenization temperature after isochoric cooling and equation of state of H_2O (Wagner and Pruß 2002).

560

561

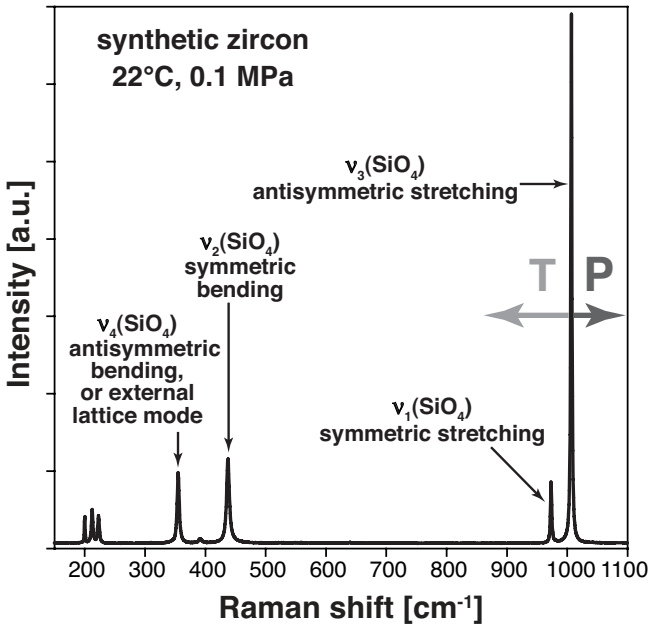
synthetic zircon
22°C, 0.1 MPa
$\nu_3(SiO_4)$
antisymmetric stretching
$\nu_2(SiO_4)$
symmetric
bending
T P
$\nu_4(SiO_4)$
antisymmetric
bending,
or external
lattice mode
$\nu_1(SiO_4)$
symmetric stretching
Intensity [a.u.]
200 300 400 500 600 700 800 900 1000 1100
Raman shift [cm^{-1}]

Fig. 1

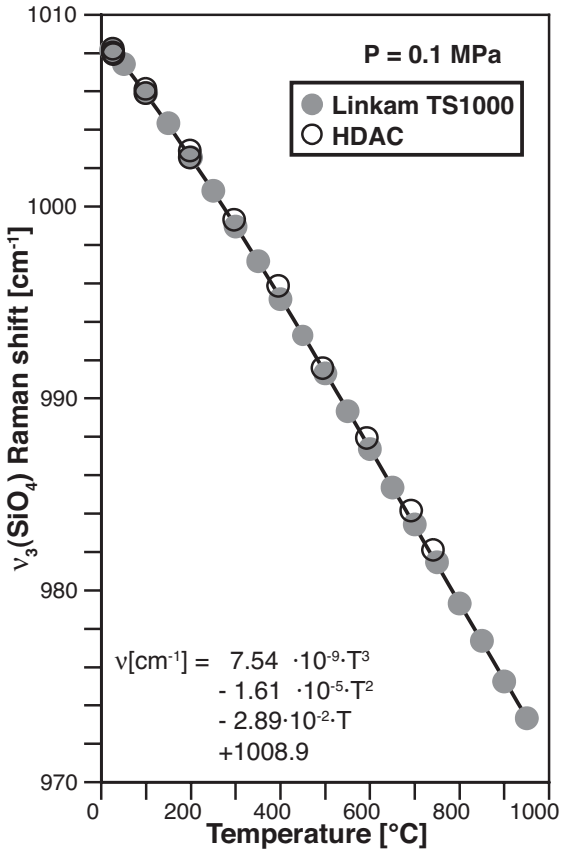
P = 0.1 MPa
Linkam TS1000
HDAC
$\nu_3(SiO_4)$ Raman shift [cm^{-1}]
Temperature [°C]
1010
1000
990
980
970
0
200
400
600
800
1000
ν[cm^{-1}] = 7.54 ·10^{-9}·T^3
- 1.61 ·10^{-5}·T^2
- 2.89·10^{-2}·T
+1008.9

Fig. 2

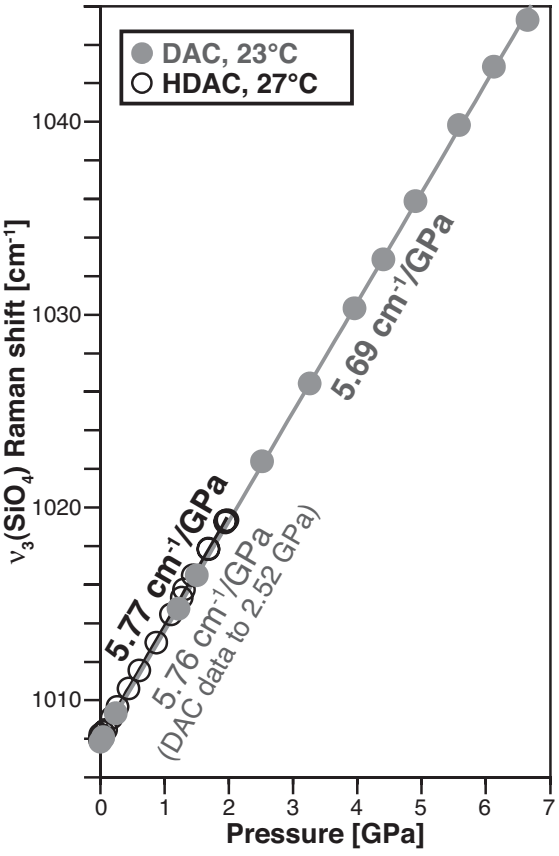
DAC, 23°C
HDAC, 27°C
5.77 cm-1/GPa
5.76 cm-1/GPa
(DAC data to 2.52 GPa)
5.69 cm-1/GPa
ν3(SiO4) Raman shift [cm-1]
Pressure [GPa]
1010
1020
1030
1040
0
1
2
3
4
5
6
7

Fig. 3

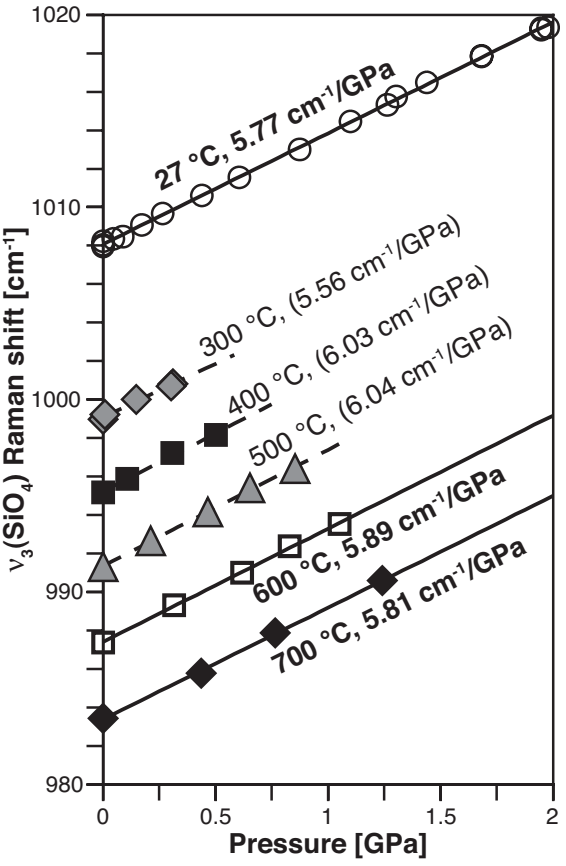
1020
1010
1000
990
980
0
0.5
1
1.5
2
$\nu_3(SiO_4)$ Raman shift [cm^{-1}]
Pressure [GPa]
27 °C, 5.77 cm^{-1}/GPa
300 °C, (5.56 cm^{-1}/GPa)
400 °C, (6.03 cm^{-1}/GPa)
500 °C, (6.04 cm^{-1}/GPa)
600 °C, 5.89 cm^{-1}/GPa
700 °C, 5.81 cm^{-1}/GPa

Fig. 4

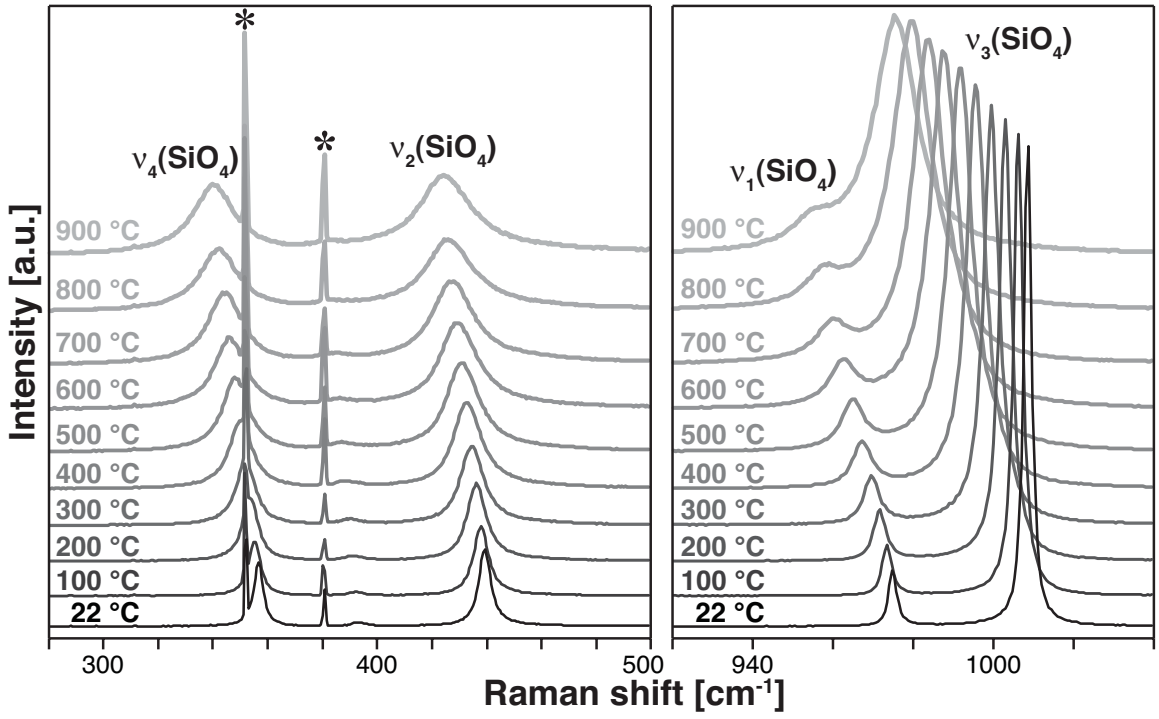
Intensity [a.u.]
$\nu_4(SiO_4)$
$\nu_2(SiO_4)$
$\nu_1(SiO_4)$
$\nu_3(SiO_4)$
*
*
900 °C
800 °C
700 °C
600 °C
500 °C
400 °C
300 °C
200 °C
100 °C
22 °C
300
400
500
940
1000
Raman shift [cm^{-1}]

Fig. 5

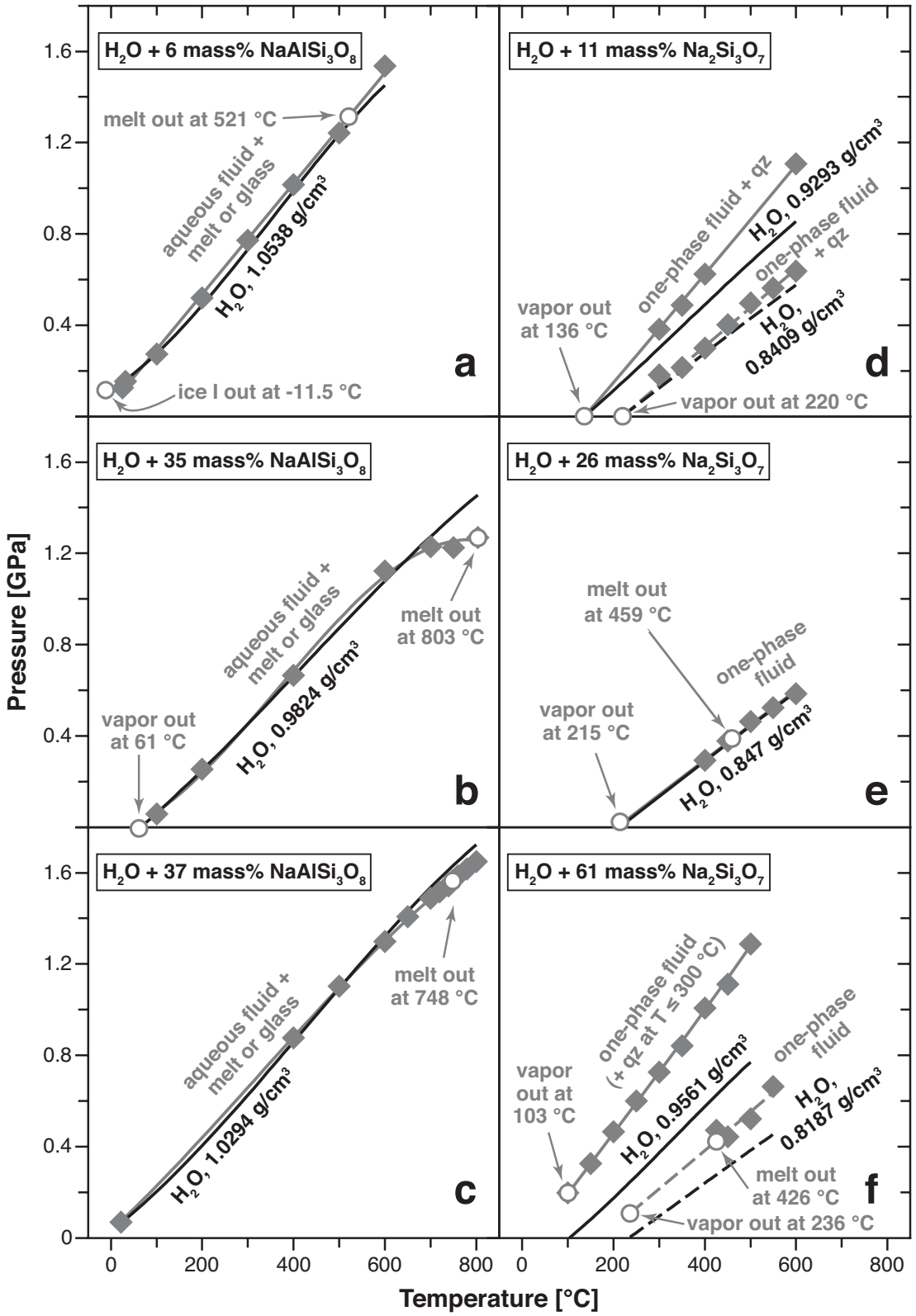
H2O + 6 mass% NaAlSi3O8
melt out at 521 °C
aqueous fluid + melt or glass
H2O, 1.0538 g/cm3
ice I out at -11.5 °C
a
H2O + 11 mass% Na2Si3O7
one-phase fluid + qz
H2O, 0.9293 g/cm3
one-phase fluid + qz
H2O, 0.8409 g/cm3
vapor out at 136 °C
vapor out at 220 °C
d
H2O + 35 mass% NaAlSi3O8
aqueous fluid + melt or glass
H2O, 0.9824 g/cm3
melt out at 803 °C
vapor out at 61 °C
b
H2O + 26 mass% Na2Si3O7
melt out at 459 °C
one-phase fluid
vapor out at 215 °C
H2O, 0.847 g/cm3
e
H2O + 37 mass% NaAlSi3O8
aqueous fluid + melt or glass
melt out at 748 °C
H2O, 1.0294 g/cm3
c
H2O + 61 mass% Na2Si3O7
one-phase fluid (+ qz at T ≤ 300 °C)
H2O, 0.9561 g/cm3
one-phase fluid
H2O, 0.8187 g/cm3
vapor out at 103 °C
melt out at 426 °C
vapor out at 236 °C
f
Pressure [GPa]
Temperature [°C]
0
0.4
0.8
1.2
1.6
200
400
600
800

Fig. 6